EFFECT OF STRUCTURAL NONLINEARITIES ON AEROELASTIC STABILITY OF A WING-PROPELLER SYSTEM

Giacomo Lazzaro
Politecnico di Milano
Milano, Italy

Giuseppe Quaranta
Politecnico di Milano
Milano, Italy

Vincenzo Muscarello
RMIT University
Melbourne, VIC, Australia

ABSTRACT

This paper investigates the impact of freeplay nonlinearity on the aeroelastic stability of a wing–propeller system representative of an electric Vertical Take-Off and Landing (eVTOL) vehicle. The freeplay is introduced in the propeller tilting mechanism, affecting the pitch degree of freedom. Stability analyses are carried out in airplane mode, using freestream velocity as the primary parameter. The study begins with the standalone propeller–pylon system and is subsequently extended to the complete configuration, including wing structural dynamics. The analysis employs a multibody dynamics framework coupled with a mid-fidelity aerodynamic solver based on the vortex particle method. Bifurcation diagrams reveal the emergence of limit cycle oscillations in pre-flutter conditions, underscoring their potential impact on the fatigue life of system components.

INTRODUCTION

The design of electric Vertical Take-Off and Landing (eVTOL) aircraft commonly incorporates Distributed Electric Propulsion (DEP) systems, featuring multiple propellers distributed along the wingspan. These configurations create highly flexible dynamic systems prone to aeroelastic instabilities. A common solution involves using tiltable propellers to enable vertical take-off and landing. However, repeated operational cycles can degrade the tilting mechanisms, introducing non-nominal conditions and nonlinear behaviors such as freeplay, which can significantly affect flutter clearance.

Structural nonlinearities have been extensively studied within the fixed-wing community, especially when considering freeplay on aircraft control surfaces (Ref. 1). Recently, similar studies related to pylon-store and rotor-nacelle systems emerged (Ref. 2). Indeed, with the development of tiltrotors (Refs. 3–5) and eVTOLs (Refs. 6–8), a tilting mechanism is required to rotate the proprotors (or the propellers) and the engines during the different flight phases. Repeated operational cycles can therefore cause wear and deterioration. The resulting freeplay gap and its effect on flutter clearance must be investigated to assess the impact of this nonlinearity on the vehicle's aeroelastic stability.

Mair et al. (Refs. 9, 10) employed two models representing propeller and proprotor whirl flutter to analyze the effects of structural nonlinearities using Continuation and Bifurcation Methods (CBM). Smooth and non-smooth freeplay nonlinearities have been demonstrated to significantly impact the whirl flutter characteristics of both systems, leading to the creation of several whirl flutter solution branches. Quintana et al. (Refs. 11, 12) examined the effects of gap freeplay in a propeller-pylon system under both symmetric and asymmetric conditions. Their study demonstrated that the initial gap size for discontinuities significantly influences the bifurcation diagrams, leading to variations in the critical flutter velocity.

The models developed are often simplistic, akin to early 1960s models like those of Reed et al. (Ref. 13), which primarily focused on propeller whirl flutter. Effective aeroelastic analysis of tiltrotors, however, requires accounting for wing dynamics together with proprotor aeromechanics (Ref. 14). Despite these differences, the primary instability mechanism in both cases remains whirl flutter. Recent studies by Böhnisch et al. (Ref. 15) demonstrated that the main aeroelastic phenomenon in a slender wing-propeller system representative of a tiltrotor eVTOL is wing flutter rather than whirl flutter. These findings remain consistent even when multiple propellers are integrated (Ref. 16).

The present work aims to investigate the impact of structural nonlinearities on a wing-propeller system, considering a freeplay gap on the propeller tilting mechanism. The problem is addressed using multibody models in MBDyn, an open-source tool developed at Politecnico di Milano (Ref. 17), coupled with the mid-fidelity aerodynamic solver DUST (Ref. 18). Bifurcation diagrams are generated to predict Limit Cycle Oscillations (LCOs) and identify critical pre-flutter conditions, emphasizing their potential to reduce the fatigue life of system components.

The paper begins by presenting the modeling framework and simulation tools used for the aeroelastic analysis. This is followed by a discussion of the results, starting with the isolated propeller–pylon system and then extending to the complete wing–propeller configuration, both incorporating freeplay nonlinearity in the pitch degree of freedom of the actuation system. The paper concludes with final remarks and key findings.

DYNAMIC MODEL SETUP

Methodology

Aeroelastic stability is assessed via nonlinear time-domain simulations using a coupled MBDyn–DUST toolchain. MBDyn is an open-source multibody dynamics solver supporting both rigid and flexible body modeling via differential-algebraic equations. It incorporates various A/L-stable integration schemes and features an aerodynamic module based on blade element theory, utilizing a three-state dynamic inflow model (Refs. 19, 20). DUST is a potential-flow solver employing a free-wake vortex particle method. It supports multiple aerodynamic representations—lifting lines, vortex lattice elements, and surface panels—enabling high-fidelity modeling of complex configurations with strong aerodynamic interactions. The Lagrangian grid-free formulation avoids volumetric meshing, and computational efficiency is achieved via a Cartesian fast multipole method (Refs. 21, 22). Coupling is performed using the open-source library PreCICE (Ref. 23), which enables strong two-way coupling through efficient inter-solver data exchange (Ref. 24). This framework has been validated in aeroelastic simulations of fixed- and rotary-wing systems, including tiltrotors (Ref. 25) and eVTOLs (Refs. 15, 26).

Frequencies and damping ratios are extracted from the time histories using the matrix pencil estimation (MPE) (Ref. 27). Bifurcation diagrams are also obtained from the MBDyn-DUST time histories. To maintain consistency with previously published studies, the legend for bifurcation analysis adopted in Table 1 follows the notation and classification introduced in the work of Mair et Al. (Ref. 10). This choice ensures comparability between the present results and those found in the literature, facilitating a more direct interpretation of the findings and their implications.

Graphic	Symbol	Description
△	Green triangle	Stable equilibrium
- - - -	Dashed magenta line	Unstable equilibrium
△	Blue triangle	Stable periodic solution
□	Hollow square	Hopf bifurcation

Table 1: Key to symbols and line colours used in bifurcation diagrams (Ref. 10).

Wing-Propeller Model

The wing–propeller model used in this study is based on the work of Böhnisch et al. (Refs. 15, 16). Table 2 sums up the structural and inertia properties of the wing.

Description	Value	Unit
Semispan	5.7	m
Chord, c	1.25	m
Elastic axis	0.35c	-
Center-of-gravity axis	0.46c	-
In-plane stiffness, EI_c	1.16e7	Nm^2
Out-of-plane stiffness, EI_b	2.90e6	Nm^2
Torsional stiffness, GJ	2.70e5	Nm^2
Mass/unit span	18	kg/m
Inertia/unit span	4.5	kg · m

Table 2: Generic wing properties.

The structural model of the wing is implemented in MBDyn. Its natural frequencies and mode shapes under wind-off conditions are compared with those obtained using SDBox, the frequency-domain aeroelastic solver developed by Böhnisch et al. (Ref. 15). As shown in Table 3, the results exhibit excellent agreement.

Mode	Description	SDBox [15]	MBDyn
1	1^{st} Bending OOP†	6.75	6.70
2	1^{st} Torsion	10.96	10.85
3	1^{st} Bending IP‡	13.79	13.37
4	2^{nd} Torsion	30.33	29.95

Table 3: Eigenfrequencies of the baseline wing in wind-off conditions. †: Out of plane. ‡: In plane.

The aeroelastic model of the wing is obtained by coupling the multibody model with the unsteady aerodynamics of DUST. The wing geometry is modeled using surface panels, with a discretization of 30 panels along the span and 20 along the chord. A symmetric NACA0012 airfoil is used throughout. The flutter behavior of the isolated wing is validated through time marching analyses. Figure 1 depicts the vertical displacements measured at the wing tip at different freestream velocities, showing an unstable response for $V_\infty \geq 95$ m/s, with a frequency of 8.7 Hz. The corresponding flutter speed obtained in SDBox (Ref. 15) is 93 m/s, at 9.1 Hz.

Similarly, the generic propeller presented by Böhnisch et al. (Ref. 15) is modeled in the coupled MBDyn-DUST simulation environment. The characteristics of the propeller are listed in Table 4.

The propeller operates at a constant rotational speed - Ω = 2500 rpm - and a variable collective pitch angle, fundamental to ensure the windmilling condition whenever the main continuation parameter of this study, i.e., the freestream velocity V_∞, is varied. Propeller performances are obtained in MBDyn (strip theory) and DUST (lifting line), compared with the results of (Ref. 15) in Fig. 2. A tip-loss factor and empirical

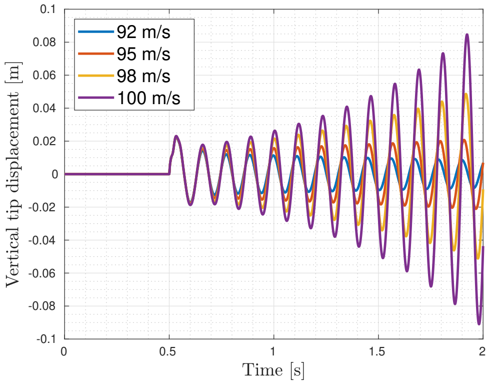

(a) MBDyn-DUST Model

Figure 1: Aeroelastic response of the wing at four freestream velocities.

Description	Value	Unit
Number of blades	4	-
Radius, R	0.9	m
Chord, c	0.22	m
Blade mass, m_B	2.2	kg
Motor mass, m_M	25	kg
Mass moment of inertia, $I_x^{(PP)}$	2.38	kg·m^2
Mass moment of inertia, $I_{y/z}^{(PP)}$	4.85	kg·m^2
Distance PP-Hub, x_H	0.4	m
Distance PP-Motor, x_M	0.3	m

Table 4: Generic propeller properties.

coefficients on the induced velocity have been used within the strip theory of MBDyn to improve the correlation with DUST and the reference data.

The tuned multibody model in MBDyn, along with the corresponding DUST model, shows excellent agreement with the reference values. Stability maps were generated to identify the whirl flutter boundaries using the two aeroelastic models developed in MBDyn and the coupled MBDyn–DUST framework. Whirl flutter conditions have been identified by varying the mounting stiffness in pitch and yaw, with the propeller operating in windmilling conditions, at freestream velocity of V_∞ = 106.5 m/s, and a rotational speed of Ω = 2500 rpm. The results show strong agreement with those reported by Böhnisch et al. (Ref. 15), as illustrated in Fig. 3.

With the isolated wing and propeller models validated independently, the integrated wing–propeller system can now be assembled. Figure 4 presents the configuration used in the subsequent analysis: the structural model implemented in MBDyn is shown in Fig. 4a, while Fig. 4b depicts the aerodynamic representation in DUST, which also serves as the aerodynamic skin in the coupled DUST–MBDyn model.

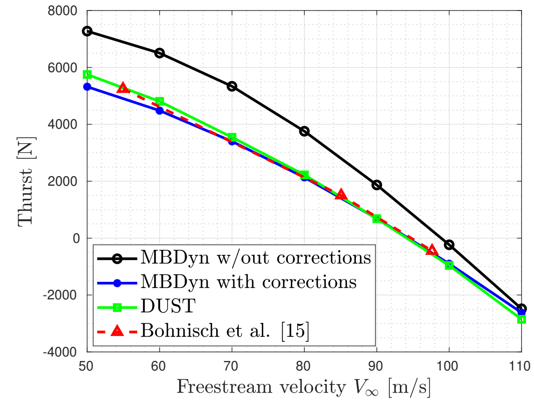

(a) Thrust.

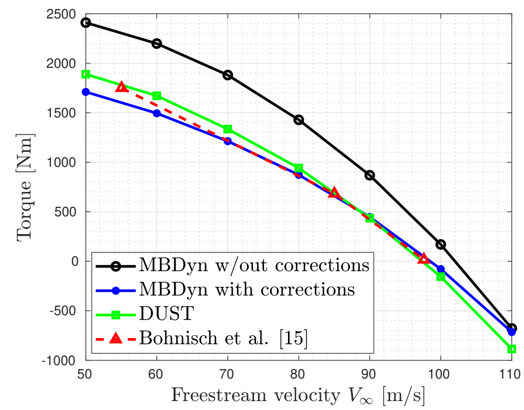

(b) Torque.

Figure 2: Propeller performance.

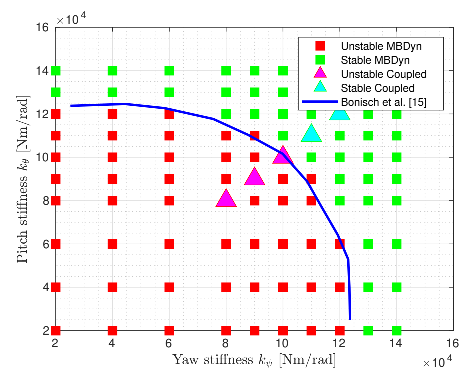

Figure 3: Propeller-pylon stability maps.

Freeplay Nonlinearity

The freeplay nonlinearity is described by a piece-wise function, namely:

$$M = \begin{cases} 0 & if \ |\theta| \leq \delta \\ k_\theta & if \ |\theta| > \delta \end{cases} \tag{1}$$

This law is highly discontinuous, as illustrated in Fig. 5. The key parameters are the deadband gap δ, defining the range over which the restoring moment is zero, and the pitch stiffness k_θ, which applies outside this zero-moment region.

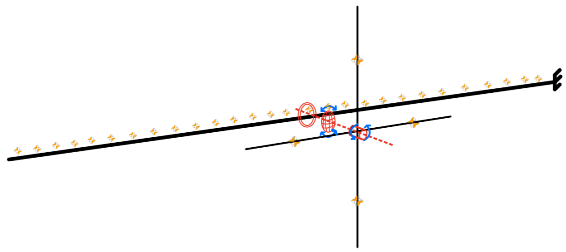

(a) MBDyn model.

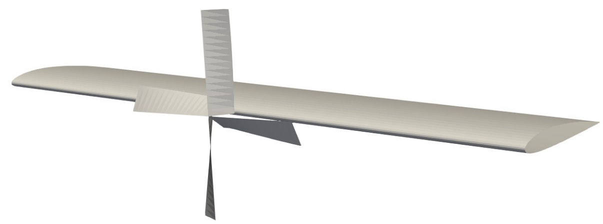

(b) DUST model.

Figure 4: Wing-propeller model: structural model in MBDyn 4a and aerodynamic model in DUST 4b.

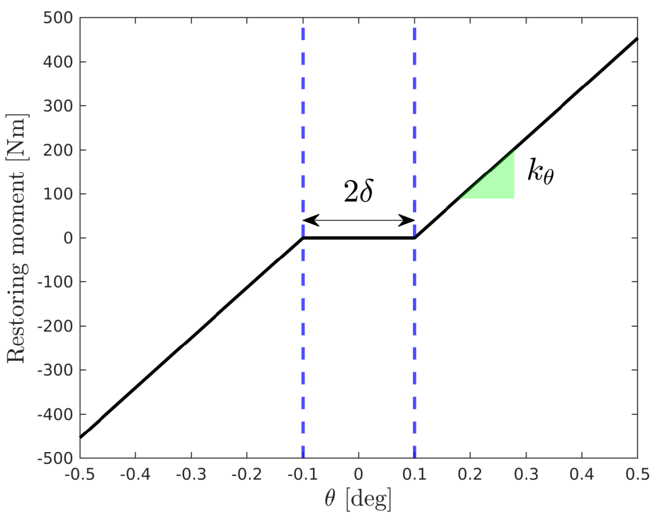

Figure 5: Freeplay constitutive law.

The freeplay nonlinearity is modeled with a gap of $\delta = 0.1°$, representing a realistic deadband width typically observed in conversion mechanisms (Ref. 10). A constant stiffness of $k_\theta = 6.5 \times 10^4$ Nm/rad is applied outside the gap, matching the nominal value used by Böhnisch et al. (Ref. 15) in their linear aeroelastic stability analysis of the wing–propeller system. The decision to model the freeplay nonlinearity exclusively in the pitch degree of freedom is motivated by the desire to capture nonlinearity only where it is physically justified. Specifically, actuation and the associated conversion mechanisms are implemented solely along the pitch axis to enable VTOL maneuvers, making it the only realistic source of mechanical freeplay.

RESULTS

Stability of the Propeller-Pylon System

The analysis begins with the standalone propeller–pylon model without freeplay to investigate the onset of whirl flutter, using freestream velocity as the primary continuation parameter. The in-vacuo eigenfrequencies and mode shapes obtained from the MBDyn model are compared with analytical results from the 2-DOF model by Reed et al. (Refs. 13, 28). Assuming a nominal rotational stiffness of 6.5×10^4 Nm/rad in both pitch and yaw at the pivot point, the characteristic backward and forward whirl modes are clearly identified. A comparison of the computed eigenfrequencies is provided in Table 5.

	Analytical [Hz]	MBDyn [Hz]
Backward whirl	10.82	10.86
Forward whirl	31.24	31.26

Table 5: Isolated propeller frequencies comparison.

To assess the linear aeroelastic stability of the propeller model, a series of time-marching simulations are performed using the MBDyn framework across a range of freestream velocities from 10 to 100 m/s, maintaining the same configuration as previously described. For each velocity, the collective pitch angle is adjusted to ensure the windmilling condition is met and the system is excited with a blended impulse force applied at the propeller hub at 0.5 seconds. Figure 6 presents the resulting stability analysis, obtained by applying the MPE method to the time histories from each simulation. The onset

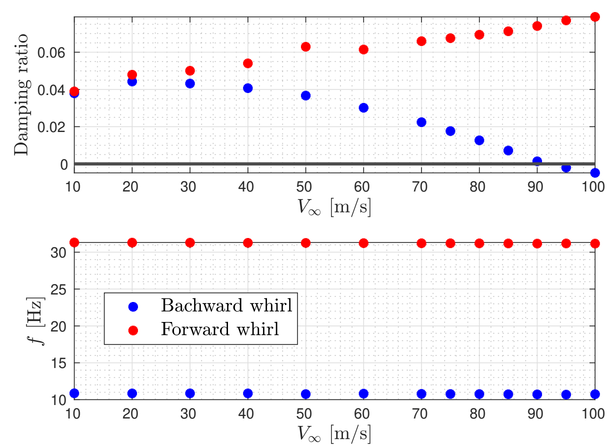

Figure 6: Stability analysis of the propeller model in MBDyn.

of instability is observed at approximately 92 m/s, where the damping ratio of the backward whirl mode crosses zero and becomes negative.

To validate this behavior, time-domain simulations were conducted using the coupled MBDyn–DUST model at two freestream velocities near the whirl flutter onset predicted by MBDyn. The resulting dynamic response, including hub motion and pitch angle over time, captures the evolution of the instability. Figure 7 illustrates the system's behavior, highlighting the emergence of unstable dynamics.

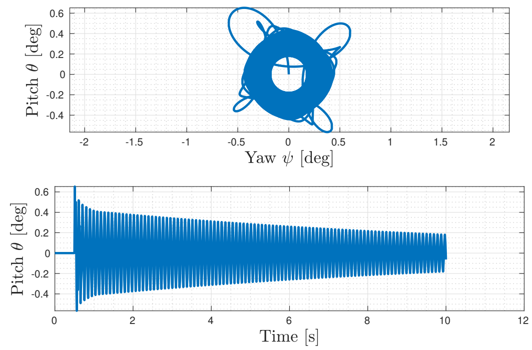

(a) Time history at 88 m/s.

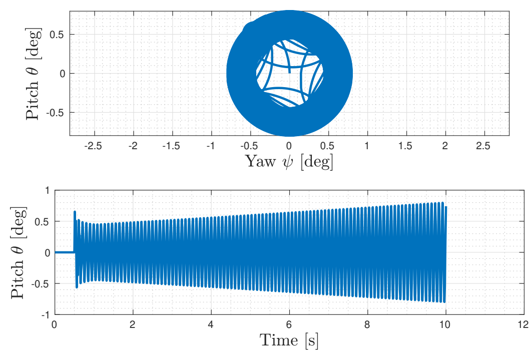

(b) Time history at 90 m/s.

Figure 7: Propeller time marching simulations in MBDyn-DUST.

The instability can be assumed at $\approx$ 89 m/s, in strong agreement with the MBDyn results. The discrepancy from the standalone MBDyn results—remaining within a 5% margin—can be attributed to the unsteady aerodynamic modeling in DUST and the influence of the wake. This again highlights DUST's tendency to yield more conservative results compared to steady or quasi-steady aerodynamic models, as previously noted by Koch et al. (Ref. 29).

The freeplay nonlinearity is therefore introduced in the MBDyn model, and the corresponding effects on the aeroelastic stability of the propeller-pylon system are depicted in the bifurcation diagram of Fig. 8. Up to 82 m/s, the pylon remains stably positioned at the edge of the deadband zone ($\theta = 0.1°$), where the non-zero structural restoring moment balances the aerodynamic loads. Beyond this point, a Hopf bifurcation occurs, giving rise to a stable LCO, indicative of attracting whirl flutter motion. The oscillation initially appears at low frequency, but increases with freestream velocity, progressively approaching the backward whirl flutter frequency. Compared to the linear case, LCOs emerge at lower speeds than the linear stability boundary. As velocity increases, the amplitude of the LCOs also grows due to the intensified aerodynamic moments. Beyond 93 m/s, the system becomes unstable and the response diverges.

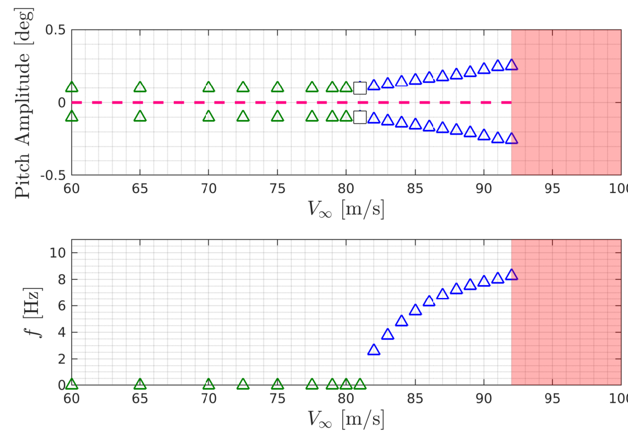

Figure 8: Bifurcation diagram of the propeller-pylon model in MBDyn.

The bifurcation diagram is then derived from simulations of the coupled MBDyn–DUST model, thereby incorporating the unsteady aerodynamics captured by DUST (see Fig. 9). As a result, the Hopf bifurcation is predicted earlier, at approximately 75 m/s. The LCO frequency gradually increases from 8 Hz to 10 Hz. At a freestream velocity of around 95 m/s, the system exhibits unstable behavior, characterized by unbounded growth in the pitch oscillation amplitude at a frequency of 10.7 Hz, closely matching the backward whirl mode. In the vicinity of the bifurcation onset, more simulations should be done to understand the phenomenon. These observations indicate that the presence of freeplay nonlinearity gives rise to a supercritical Hopf bifurcation in the pre-flutter regime, resulting in the onset of stable LCOs. It is important to note that, within the velocity range preceding the Hopf bifurcation, the presence of the freeplay gap alters the steady-state thrust direction. Rather than remaining aligned

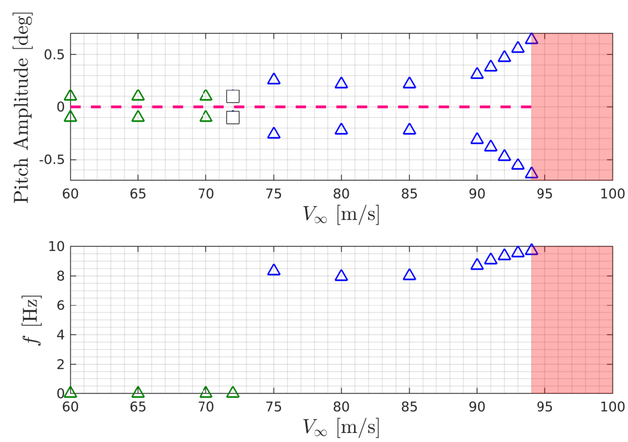

Figure 9: Bifurcation diagram of the propeller-pylon model in MBDyn-DUST.

with the freestream velocity—as expected under nominal conditions—the thrust vector deviates, potentially influencing the wing's static deformation. Finally, the last interesting observation is that the coupled model predicted instability at 89 m/s for the linear model, while the nonlinear model enters the instability region at a velocity of 95 m/s, although it already exhibits LCOs at lower velocities.

Stability of the Wing-Propeller System

After evaluating the standalone propeller–pylon system under both linear and nonlinear regimes, it is integrated onto the wing at the 50% spanwise location. The linear aeroelastic stability of the wing–propeller model is first analyzed, excluding the effects of freeplay. Table 6 reports the first four elastic eigenmodes of the complete model under wind-off conditions. The corresponding frequencies and damping ratios in MBDyn are extracted using the MPE method applied to decaying time histories and are compared with those obtained using SDBox, showing excellent agreement. Notably, the wing model includes structural damping through a stiffness-proportional damping factor, following the approach adopted by Böhnisch et al. (Ref. 15).

Description	SDBox [15]		MBDyn	
	Freq. [Hz]	ξ [%]	Freq. [Hz]	ξ [%]
Mode #1	6.26	1.81	6.21	1.81
Mode #2	6.96	1.82	6.94	1.81
Mode #3	12.58	3.70	12.19	3.67
Mode #4	14.78	1.83	14.62	1.72

Table 6: Eigenfrequencies of baseling wing-propeller model in wind-off conditions.

Following the structural validation, the flutter boundaries of the complete aeroelastic model are assessed as a final benchmark before advancing with further model development. The stability analysis is conducted under linear conditions using the coupled MBDyn–DUST framework. To excite both out-of-plane bending and torsional dynamics, a blended impulse force of 12 kN is applied 2 ms before the elastic axis at the wing tip. The flutter conditions are summarized in Table 7.

Description	SDBox [15]	MBDyn-DUST
V_∞ [m/s]	150	155
Freq. [Hz]	11.2	11.6

Table 7: Flutter point of the wing-propeller system.

For this configuration, the flutter mechanism emerges at a velocity slightly above 150 m/s with a frequency of 11.6 Hz, consistent with the SDBox simulation results from (Ref. 15). According to SDBox, the third eigenmode that becomes unstable involves a combination of torsion, in-plane bending, and a backward whirl motion that is out of phase with the wing. Examination of the time-marching simulation frames reveals the same mode shape in the MBDyn–DUST model. A frame illustrating this unstable aeroelastic mode, taken from (Ref. 15), is shown in Figure 10.

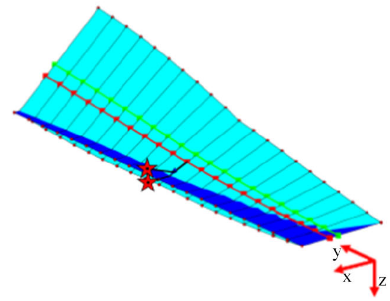

Figure 10: Unstable aeroelastic mode (Ref. 15).

In the following analysis, bifurcation diagrams are generated by introducing freeplay in the pitch mounting stiffness. The absolute amplitude of the pitch angle measured at the propeller hub and the corresponding frequency of the resulting limit cycle oscillations are presented in Fig. 11.

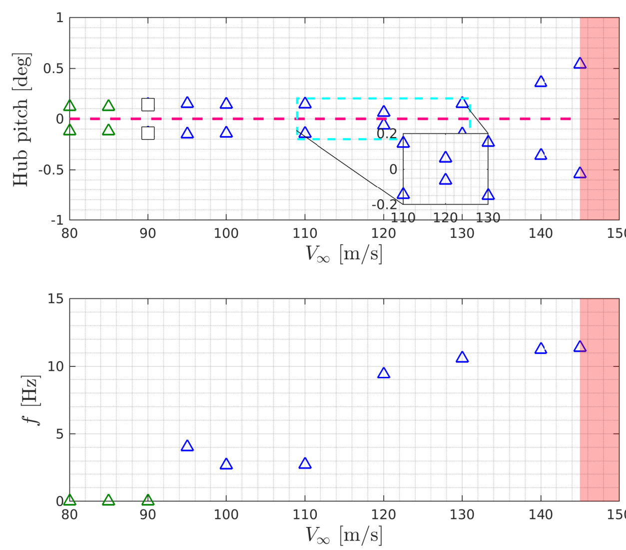

Figure 11: Bifurcation diagram of the wing-propeller model in MBDyn-DUST: hub pitch.

The bifurcation diagram shows that up to V_∞ = 90 m/s, the system stabilizes at an equilibrium near the edge of the deadband zone. The blockage occurs at a pitch angle slightly above 0.1°, though this angle also reflects the wing's static deformation caused by the propeller's offset from the flow alignment. As velocity increases, a Hopf bifurcation appears: at 95 m/s, the system exhibits a chaotic response with an average frequency of approximately 4.0 Hz, indicating the onset of the instability. Increasing the speed, an LCO linked to the propeller dynamics emerges, initially at a low frequency of approximately 3 Hz. In contrast, oscillations at the wing tip remain roughly an order of magnitude smaller and occur at a different frequency, indicating that the wing's dynamics are initially decoupled from the propeller-induced LCOs, as shown in Fig. 12.

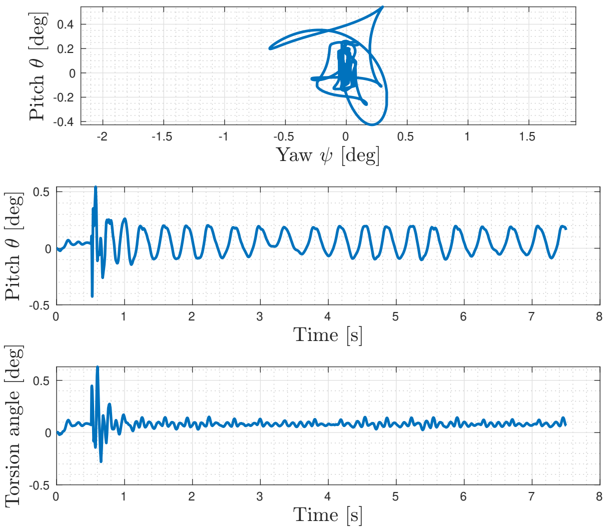

Figure 12: Time histories of the wing–propeller model simulated in MBDyn–DUST at V_∞ = 100 m/s: hub rotations (top), hub pitch angle (middle), and wing torsional deformation (bottom).

As the freestream velocity reaches $V_\infty = 120$ m/s, the amplitude of the propeller LCO decreases, while the frequency increases. This behavior is highlighted in the zoomed inset of Fig. 11. At this stage, the wing dynamics begin to play a role in the overall response, as indicated by the increase in torsional oscillation amplitude at the wing tip, shown in Fig. 13.

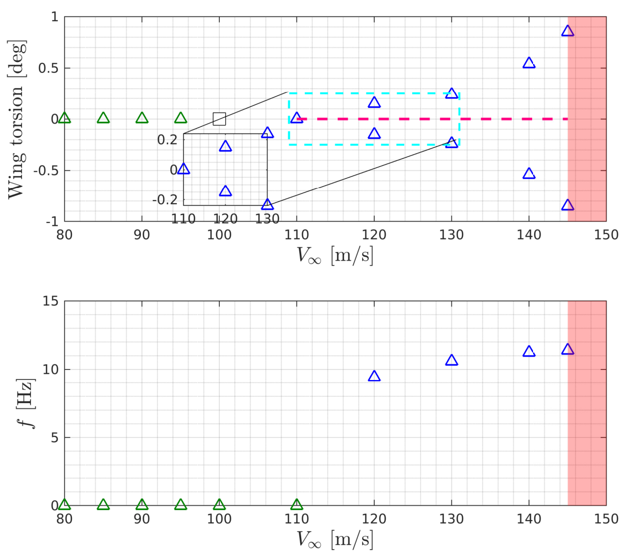

Figure 13: Bifurcation diagram of the wing-propeller system in MBDyn-DUST: wing torsion.

The frequency increases to approximately 10 Hz, leading to dynamic coupling with the wing's third eigenmode. This mode involves a combination of wing torsion, in-plane bending, and a backward whirl motion. The observed reduction in the hub pitch amplitude is a result of this coupling. Specifically, the backward whirl mode is out of phase with the wing torsion—meaning that a positive torsional peak in the wing corresponds to a negative peak in the hub pitch angle. This out-of-phase interaction limits the absolute amplitude of the hub oscillation. Fig. 14 clearly illustrates the 180 deg. phase shift between the wing torsion and the hub pitch oscillations.

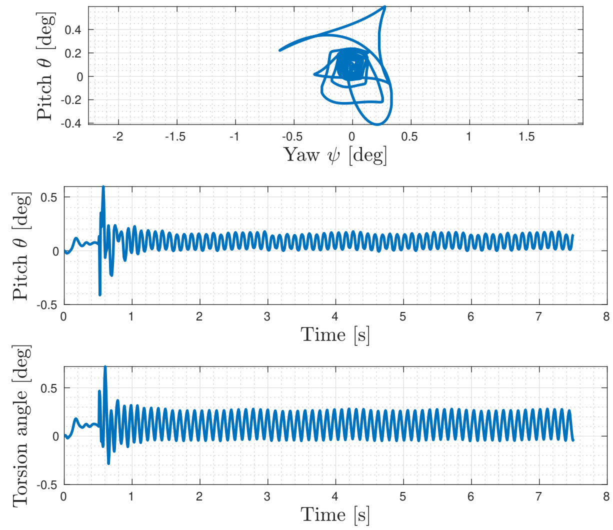

Figure 14: Time histories of the wing–propeller model simulated in MBDyn–DUST at V_∞ = 120 m/s: hub rotations (top), hub pitch angle (middle), and wing torsional deformation (bottom).

As the speed continues to increase, the pitch oscillation amplitudes begin to grow again, with the frequency approaching 11.9 Hz—matching the predicted flutter frequency. Although the freeplay is applied only in the pitch degree of freedom, larger oscillations also develop in the yaw direction at higher flight speeds. This behavior results from gyroscopic effects and aerodynamic forces coupling the propeller pitch and yaw motions, as illustrated in Fig. 15. Ultimately, at $V_\infty = 150$ m/s, the system exhibits a divergent response, occurring slightly below the flutter speed predicted by the model without freeplay.

CONCLUSIONS

1. In the standalone propeller–pylon system, the presence of freeplay affects the steady-state solution as a function of flight speed. At low speeds (up to approximately 75–80 m/s), the stable equilibrium shifts from the undeformed position to the edge of the deadband zone—either the upper or lower limit—depending on the initial conditions. As the speed increases further, LCOs emerge at a velocity lower than the whirl flutter speed predicted by linear analysis. The frequency of these LCOs increases with flight speed, eventually approaching the backward whirl frequency, which leads to divergent oscillations.

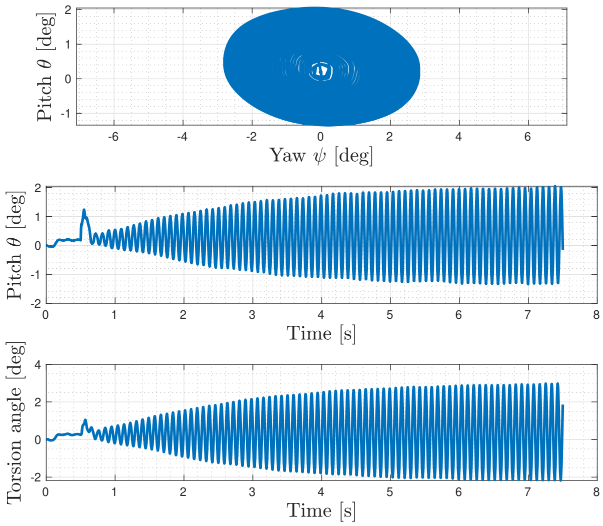

Figure 15: Time histories of the wing–propeller model simulated in MBDyn–DUST at $V_\infty = 150$ m/s: hub rotations (top), hub pitch angle (middle), and wing torsional deformation (bottom).

Similar behavior is observed in both standalone MBDyn simulations and in the coupled MBDyn–DUST simulation environment. However, the MBDyn–DUST coupling tends to produce more conservative results, predicting the onset of LCOs at lower speeds and with higher amplitudes compared to MBDyn alone.

2. A consistent pattern is observed in the complete wing–propeller model at flight speeds below 120 m/s, where wing deformations remain limited. Beyond this range, the wing's dynamics begin to influence the LCOs on the propeller. As the speed increases, the LCO frequency approaches that of the wing's third mode. Initially, the amplitude of hub oscillations decreases, as the wing's torsional response appears at the same frequency but out of phase with the propeller's backward mode. However, the amplitude later increases again, eventually triggering wing flutter. The flutter instability occurs at a speed that closely matches the prediction from linear analysis ($\approx$ 150 m/s). Notably, the irregular onset of LCOs around 95 m/s suggests the presence of complex, possibly chaotic dynamics near the bifurcation point. This region warrants further investigation through additional simulations to fully understand the system's behavior.

3. In conclusion, introducing freeplay in the pitch motion of the propeller–pylon system reduces the stability margins in both the standalone configuration and the complete wing–propeller system. In both cases, limit cycle oscillations (LCOs) emerge at flight speeds significantly lower than those predicted by linear stability analysis. Although the oscillation amplitudes remain small—typically less than 1 degree when the freeplay gap is 0.1 degree—they can still have a meaningful impact on the fatigue life of the wing–propeller system.

4. Future analyses will need to investigate the sensitivity of stability margins to variations in the freeplay gap and how these changes affect the bifurcation behavior. The study will also be extended to consider different positions of the propeller–pylon system along the wing semispan.

Author contact:
Giacomo Lazzaro giacomo.lazzaro@polimi.it
Giuseppe Quaranta giuseppe.quaranta@polimi.it
Vincenzo Muscarello vincenzo.muscarello@rmit.edu.au

ACKNOWLEDGMENTS

Funded by Unione Europea - Next Generation EU, Missione 4 Componente 1 CUP D43C23002610001.

REFERENCES

1. Panchal, J., and Benaroya, H., "Review of control surface freeplay," *Progress in Aerospace Sciences*, Vol. 127, 2021. DOI: 10.1016/j.paerosci.2021.100729.

2. Xu, Y., Cao, D., Lin, H., and Shao, C., "An alternative simulation approach for the ONERA aerodynamic model and its application in the nonlinear aeroelastic analysis of slender wings with pylon-store system," *International Journal of Non-linear Mechanics*, Vol. 105, 2018, pp. 55–76. DOI: https://doi.org/10.1016/j.ijnonlinmec.2018.07.003.

3. White, G., "A tilt-rotor actuator," *Proceedings of the Institution of Mechanical Engineers Part G Journal of Aerospace Engineering*, Vol. 224, 2010, pp. 657–672. DOI: https://doi.org/10.1243/09544100JAERO666.

4. Sanchez-Rivera, L. M., Lozano, R., and Arias-Montano, A., "Development, Modeling and Control of a Dual Tilt-Wing UAV in Vertical Flight," *Drones*, 2020. DOI: https://doi.org/10.3390/drones4040071.

5. Belardo, M., Beretta, J., Marano, A. D., Diodati, G., Paletta, N., and Di Palma, L., "On the Preliminary Structural Design Strategy of the Wing of the Next-Generation Civil Tiltrotor Technology Demonstrator," *International Journal of Aeronautical and Space Sciences*, Vol. 22, 2021, pp. 613–624. DOI: https://doi.org/10.1007/s42405-020-00330-2.

6. Muraoka, K., Okada, N., and Kubo, D., "Quad Tilt Wing VTOL UAV: Aerodynamic Characteristics and Prototype Flight Test," *AIAA InfoTech*, Seattle, WA, 2009. DOI: https://doi.org/10.2514/6.2009-1834.

7. Kiesewetter, L., Shakib, K. H., Singh, P., Rahman, M., Khandelwal, B., Kumar, S., and Shah, K., "A holistic review of the current state of research on aircraft design concepts and consideration for advanced air mobility applications," *Progress in Aerospace Sciences*, Vol. 142, 2023. DOI: https://doi.org/10.1016/j.paerosci.2023.100949.

8. Akash, A., Raj, V. S. J., Sushmitha, R., Prateek, B., Aditya, S., and Sreehari, V. M., "Design and Analysis of VTOL Operated Intercity Electrical Vehicle for Urban Air Mobility." *Electronics*, Vol. 11, 2022. DOI: https://doi.org/10.3390/electronics11010020.

9. Mair, C., Rezgui, D., and Titurus, B., "Nonlinear stability analysis of whirl flutter in a rotor-nacelle system," *Nonlinear dyn*, Vol. 94, 2018, pp. 2013–2032. DOI: https://doi.org/10.1007/s11071-018-4472-y.

10. Mair, C., Titurus, B., and Rezgui, D., "Stability analysis of whirl flutter in rotor-nacelle systems with freeplay nonlinearity," *Nonlinear dyn*, Vol. 104, 2021, pp. 65–89. DOI: https://doi.org/10.1007/s11071-021-06271-z.

11. Quintana, A., Saunders, B. E., Vasconcellos, R., and Abdelkefi, A., "Nonlinear characterization of the piecewise structural effects on whirl flutter of a rotor-nacelle system," *AIAA SciTech*, San Diego, CA, 2022. DOI: https://doi.org/10.2514/6.2022-2269.

12. Quintana, A., Saunders, B. E., Vasconcellos, R., and Abdelkefi, A., "The influence of freeplay on the whirl flutter and nonlinear characteristics of rotor-nacelle systems," *Meccanica*, Vol. 58, 2023, pp. 659–686. DOI: https://doi.org/10.1007/s11012-023-01658-1.

13. W. H. Reed and S. R. Bland, "An Analytical Treatment of Aircraft Propeller Precession Instability," *Technical Note*, Vol. D-659, 1961.

14. Masarati, P., Muscarello, V., and Quaranta, G., "Linearized Aeroservoelastic Analysis of Rotary-Wing Aircraft," 36th European Rotorcraft Forum, September 7–9 2010.

15. Böhnisch, N. and Braun, C. and Muscarello, V. and Marzocca, P., "About the Wing and Whirl Flutter of a Slender Wing-Propeller System," *Journal of Aircraft*, Vol. 61, 2024, pp. 1117–1130. DOI: https://doi.org/10.2514/1.C037542.

16. Böhnisch, N., *Exploring Aeroelastic Stability and Design Principles in AircraftWings with Distributed Propulsion Systems*, Ph.D. thesis, RMIT University, 2025.

17. Masarati, P., Morandini, M., and Mantegazza, P., "An Efficient Formulation for General-Purpose Multibody/Multiphysics Analysis," *Journal of Computational and Nonlinear Dynamics*, Vol. 9, 2014. DOI: https://doi.org/10.1115/1.4025628.

18. Savino, A., Cocco, A., Zanotti, A., Tugnoli, M., Masarati, P., and Muscarello, V., "Coupling mid-fidelity aerodynamics and multibody dynamics for the aeroelastic analysis of rotary-wing vehicles," *Energies*, Vol. 14, 2021. DOI: https://doi.org/10.3390/en14216979.

19. Pitt, D. M., and Peters, D. A., "Theoretical prediction of dynamic inflow derivatives," 6th European Rotorcraft and Powered Lift Aircraft Forum, 1980.

20. Pitt, D. M., and Peters, D. A., "Rotor Dynamic Inflow Derivatives and Time Constants from Various Inflow Models," 9th European Rotorcraft Forum, Vol. Paper No. 55, 1983.

21. Cottet, G. H., and Koumoutsakos, P. D., *Vortex methods: theory and practice*, Cambridge University Press, 2000.

22. Winckelmans, G. S., *Topics in vortex methods for the computation of three-and two-dimensional incompressible unsteady flows*, Ph.D. thesis, California Institute of Technology, 1989.

23. Chourdakis, G., Davis, K., Rodenberg, B., Schulte, M., Simonis, F., Uekermann, B., Abrams, G., Bungartz, H. J., Cheung Yau, L., Desai, I., Eder, K., Hertrich, R., Lindner, F., Rusch, A., Sashko, D., Schneider, D., Totounferoush, A., Volland, D., Vollmer, P., and Koseomur, O. Z., "preCICE v2: A sustainable and user-friendly coupling library," *Open Research Europe*, Vol. 2, (51), 2022. DOI: 10.12688/openreseurope.14445.2.

24. Savino, A., Cocco, A., Zanotti, A., Tugnoli, M., Masarati, P., and Muscarello, V., "Coupling mid-fidelity aerodynamics and multibody dynamics for the aeroelastic analysis of rotary-wing vehicles," *Energies*, Vol. 14, (21), 2021, pp. 6979.

25. Savino, A., Cocco, A., and Muscarello, V., "Evaluation of Dynamic Loads and Performance Indexes in Tiltrotors using a Mid-Fidelity Aeroservoelastic Tool," *Aerospace Science and Technology*, Vol. 146, 2024. DOI: 10.1016/j.ast.2024.108929.

26. Böhnisch, N. and Braun, C. and Marzocca, P. and Muscarello, V., "Impact of Aerodynamic Interactions on Aeroelastic Stability of Wing-Propeller Systems," *Applied Sciences*, Vol. 14, 2024. DOI: https://doi.org/10.3390/app14198709.

27. Hua, Y., and Sarkar, T. K., "Matrix Pencil Method for Estimating Parameters of exponentially Damped/Undamped Sinusoids in Noise," *IEEE Transactions on acoustics speech and signal processing*, Vol. 38, 1990, pp. 814–824. DOI: https://doi.org/10.1109/29.56027.

28. Böhnisch, N. and Kantzidis, C. and Masarati, P. and Muscarello, V., "Assessment of Aerodynamic Torque on Propeller Whirl Flutter and Its Control," *Journal of Aircraft*, 2025. DOI: https://doi.org/10.2514/1.C038128.

29. C. Koch, and N. Böhnisch, and H. Verdonck, and O. Hach, and C. Braun, "Comparison of Unsteady Low- and Mid-Fidelity Propeller Aerodynamic Methods for Whirl Flutter Applications," *Applied Sciences*, Vol. 14, 2024. DOI: https://doi.org/10.3390/app14020850.